Asian Journal of Pharmaceutical Sciences 19 (2024) 100892

Available online at www.sciencedirect.com

ScienceDirect

journal homepage: www.elsevier.com/locate/AJPS

Research Article

A natural compound-empowered podophyllotoxin prodrug nanoassembly magnifies efficacy-toxicity benefits in cancer chemotherapy

Ziqi Lin[a,1], *Yuequan Wang*[a,1], *Wenwen Li*[a], *Fei Sun*[a], *Qingzhi Lv*[d], *Shenwu Zhang*[a,b], *Xiaohong Liu*[c], *Feng Qin*[c,*], *Cong Luo*[a,b,*]

[a] *Department of Pharmaceutics, Wuya College of Innovation, Shenyang Pharmaceutical University, Shenyang 110016, China*
[b] *Joint International Research Laboratory of Intelligent Drug Delivery Systems of Ministry of Education, Shenyang Pharmaceutical University, Shenyang 110016, China*
[c] *College of Pharmacy, Shenyang Pharmaceutical University, Shenyang 110016, China*
[d] *School of Pharmacy, Binzhou Medical University, Yantai 264003, China*

ARTICLE INFO

Article history:
Received 2 January 2024
Revised 21 February 2024
Accepted 22 February 2024
Available online 28 February 2024

Keywords:
Podophyllotoxin
Prodrug
Chemosensitization
Hybrid nanoassembly
Cancer chemotherapy

ABSTRACT

Small-molecule prodrug nanoassembly technology with a unique advantage in off-target toxicity reduction has been widely used for antitumor drug delivery. However, prodrug activation remains a rate-limiting step for exerting therapeutic actions, which requires to quickly reach the minimum valid concentrations of free drugs. Fortunately, we find that a natural compound (BL-193) selectively improves the chemotherapy sensitivity of breast cancer cells to podophyllotoxin (PPT) at ineffective dose concentrations. Based on this, we propose to combine prodrug nanoassembly with chemotherapy sensitization to fully unleash the chemotherapeutic potential of PPT. Specifically, a redox-sensitive prodrug (PSSF) of PPT is synthesized by coupling 9-fluorenyl-methanol (Fmoc-OH) with PPT linked via disulfide bond. Intriguingly, PSSF with a π-conjugated structure readily co-assembles with BL-193 into stable nanoassembly. Significantly, BL-193 serves as an excellent chemosensitizer that creates an ultra-low-dose chemotherapeutic window for PPT. Moreover, prodrug design and precise hybrid nanoassembly well manage off-target toxicity. As expected, such a BL-193-empowered prodrug nanoassembly elicits potent antitumor responses. This study offers a novel paradigm to magnify chemotherapy efficacy-toxicity benefits.

* Corresponding authors.
E-mail addresses: qf-1998@163.com (F. Qin), luocong@syphu.edu.cn (C. Luo).
[1] These authors contributed equally to this work.
Peer review under responsibility of Shenyang Pharmaceutical University.

https://doi.org/10.1016/j.ajps.2024.100892

1. Introduction

Cancer continues to pose a significant risk to both human health and quality of life [1]. Numerous clinical therapeutic approaches have been devised and implemented to address this challenge, including surgical resection, chemotherapy, radiotherapy and phototherapy [2–4]. Among them, chemotherapy represents one of the most commonly used treatments by virtue of broad-spectrum anti-tumor effects and systemic therapeutic features [5–7]. However, the clinically available chemotherapeutics suffer from poor specificity, unsatisfactory treatment outcome and narrow treatment window [8]. There's urge need to develop new drugs and strategies to improve the current situation. Podophylotoxin (PPT) has attracted much attention in pre-clinical investigations. PPT showed potent antitumor activity through binding with tubulins to inhibit the formation of mitotic spindle in the process of cell division [9–11]. Disappointingly, PPT not only has poor water solubility, but also produces serious off-target toxicity. Because of this, it has not yet been used in cancer clinical treatment [12]. In the past decade, in order to overcome these shortcomings of PPT, pharmaceutical chemists have attempted to synthesize a series of analogous compounds [13,14], such as etoposide (VP-16) [15,16]. Nevertheless, despite the utilization of VP-16 in the clinical treatment of cancers such as breast cancer and leukemia, they are still criticized for poor treatment efficacy and severe toxic side effects. Obviously, in order to reduce toxicity, it had no alternative but to sacrifice certain antitumor activity when designing PPT analogues. Whereas it is necessary to retain its potent antitumor activity when considering the drug availability of PPT. In other words, it's of critical importance to guarantee antitumor activity while improving safety [17,18].

Prodrug strategy has been widely used to facilitate anticancer drug delivery [17,19-21]. A feasible prodrug strategy can handle multiple challenges from anticancer drug delivery, such as severe toxicity, lack of site specificity, and inferior cellular uptake efficiency [22]. Despite advances from conventional prodrug strategy, some weaknesses have greatly impeded their clinical translation and application [23]. Particularly, small-molecule prodrugs suffer from rapid clearance and premature degradation. In response to these challenges of conventional prodrug strategy, carrier-free prodrug nanoassembly, integrating prodrug strategy and biomedical nanotechnology into one system [24], has emerged as a notable trend to facilitate more efficient delivery of anticancer drugs in recent decades [18,25-29]. Prodrug nanoassembly confers anticancer drugs many advantages, such as improved drug availability, on-demand prodrug activation and drug release [28,30,31]. Moreover, one of the most distinct advantages of small-molecule prodrug nanoassembly over conventional nanocarrier-based nanomedicines lies in high drug loading capacity, even as high as 50% to 80%. More important, tumor-specific prodrug activation could be facilely realized by inserting tumor stimuli-sensitive chemical linkers in the conjugates, such as disulfide bond [22,32]. For instance, disulfide bond-linked prodrugs could be activated in the presence of glutathione (GSH) overproduced in tumor cells (1-10 mM), while normal cells usually have much lower GSH levels, usually 4 to 10 times lower [33–35]. In this way, the off-target toxicity of anticancer drugs could be well managed through tumor-selective prodrug activation. Nevertheless, prodrug activation remains a rate-limiting step for therapeutic actions, which requires to at least reach the minimum valid concentrations of free drugs. As a result, both prodrugs and prodrug-based nanomedicines showed relatively weaker cytotoxicity than the corresponding parent drugs. Whether the antitumor potential can be fully fulfilled has become a key problem to be solved in prodrug-based drug delivery modalities [36].

Herein, we found that a natural compound (BL-193) was able to significantly improve the chemotherapy sensitivity of breast cancer cells to podophyllotoxin (PPT), even at ineffective dose concentrations (Fig. 1). Based on this interesting finding, we proposed to develop a novel chemotherapy regimen through combining prodrug nanoassembly with chemotherapy sensitization to fully unleash the chemotherapeutic potential of PPT [37,38]. On the one hand, prodrug strategy was engaged to reduce the toxicity of PPT by introducing tumor stimuli-responsive chemical linkages in conjugate design. On the other hand, BL-193-mediated chemotherapy sensitization was expected to improve the therapeutic efficiency of PPT prodrug, especially dealing with the problem of delayed and inadequate prodrug activation. Specifically, a redox-sensitive prodrug (PSSF) of PPT was rationally designed and synthesized by coupling 9-fluorenyl-methanol (Fmoc-OH) with PPT linked via disulfide bond [39]. Intriguingly, we found that PSSF with a π-conjugated Fmoc structure readily co-assembled with BL-193 into stable nanoparticles at a wide molar ratio from 1:0 to 1:9. After nano-formulation and synergistic sensitization optimization, a precise hybrid nanoassembly of PSSF and BL-193 was fabricated at the optimal molar ratio of 1:5. In the nanoassembly, BL-193 served as an excellent chemosensitizer that opened an ultra-low-dose chemotherapeutic window for PPT. Moreover, tumor-specific prodrug design and precise hybrid nanoassembly well managed the off-target toxicity of PPT. By virtue of these advantages and characteristics, such a BL-193-empowered prodrug nanoassembly produced potent antitumor responses *in vitro* and *in vivo*. Moreover, it significantly reduced toxicity when compared with free PPT solution. To our knowledge, this marks the inaugural endeavor to construct carrier-free hybrid nanomedicine by integrating prodrug nanoassembly nanotechnology with natural chemosensitizer-empowered chemosensitization strategy, which neatly solved the prodrug activation- caused poor efficacy by a unique way of chemotherapeutic window expansion. This study offers a novel combination treatment paradigm for precision cancer chemotherapy.

2. Materials and methods

2.1. *Materials*

PPT, cell culture medium, Cyanine7 (Cy7), the reagents applied in Western blot assay were purchased from Meilun Biotech Co. Ltd. (Dalian, China). DSPE-mPEG$_{2k}$ was obtained from AVT

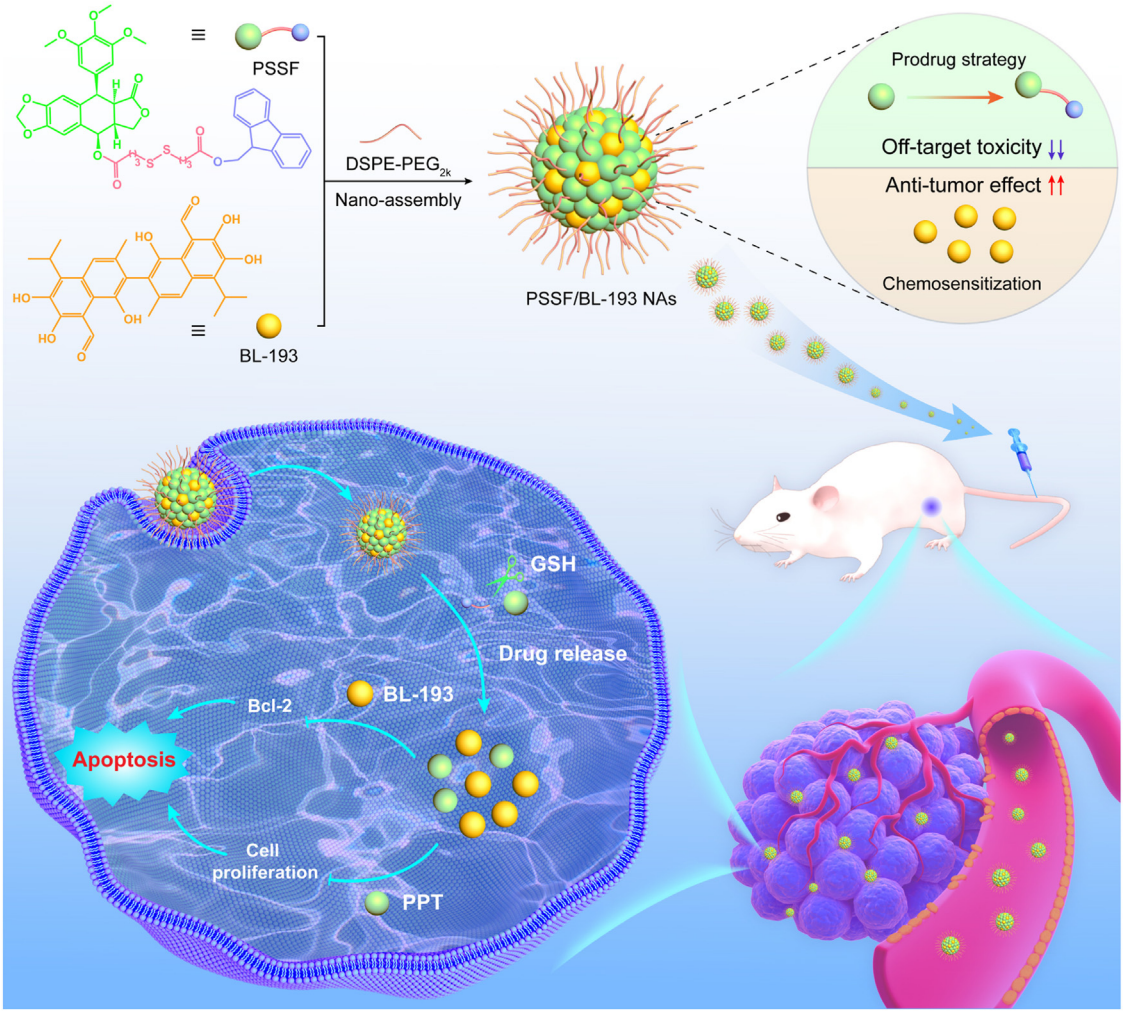

Fig. 1 – Schematic illustration of a BL-193-empowered prodrug nanoassembly elicits potent antitumor responses and reduces off-target toxicity.

(Shanghai) Pharmaceutical Technology Co., Ltd. (Shanghai, China). DSPE-mPEG$_{2K}$-Cy7 was obtained from Xi'an Ruixi Biological Technology Co., Ltd (Xi'an, China). Annexin V-FITC Apoptosis Detection Kit was obtained from was purchased from Beijing Solarbio Science & Technology Co., Ltd (Beijing, China). All the cell culture vessels were purchased from NEST Biotechnology Co., Ltd. (Wuxi, China). 4T1 cells, 3T3 cells and RM-1 cells were obtained from the ATCC. Specifically, 4T1 cells were cultivated in RPMI 1640 medium with 10% fetal bovine serum (FBS). 3T3 cells were cultivated in DMEM medium with the same components mentioned earlier. The use of animals is approved by the Animal Ethics Committee of Shenyang Pharmaceutical University (No. 19169).

2.2. *Synthesis of PPT-SS-Fmoc prodrugs*

To enhance the esterification activity of dithioglycolic acid, we stirred 4,4′-dithioglycolic acid (1 mmol) in 3 ml acetic anhydride under nitrogen protection. Subsequently, we obtained 4,4′-dithiodibutyric anhydride. Next, we conducted the esterification of Fmoc-OH (1 mmol) with 4,4′-dithiodibutyric anhydride for 12 h, catalyzed by DMAP (0.1 mmol). The intermediate product activated with 1 mmol EDCI, 1 mmol HOBt, and 0.1 mmol DMAP in an ice bath for 2 h. Subsequently, we added PPT to the system and stirred it for 48 h to obtain the prodrug. We removed dichloromethane and obtained the final product using preparative liquid chromatography [39].

2.3. *Preparation and characterization of PSSF/BL-193 NAs*

PSSF/BL-193 NAs were created using a one-step nanoprecipitation method. PSSF and BL-193 were dissolved in a solution of tetrahydrofuran (THF) with a PEG concentration of 1.25 mg/ml, resulting in a mixed solution with a concentration of 2.5 mg/ml [40]. Further dilution was attained by adding anhydrous ethanol to achieve a 1:1 ethanol-to-THF ratio. Subsequently, a mixture of PSSF and BL-193 at varying molar ratios was added dropwise into 2 ml deionized water under stirring at 1,200 rpm for 2 min to prepare PSSF/BL-193 NAs at different molar ratios.

To identify the optimal dose ratio of PSSF and BL-193, both the particle size and IC_{50} values were used to screen formualtions. The sensitization effect of BL-193 on PSSF was assessed using the MTT assay. Initially, 4T1 cells were plated at a density of 2×10^3 cells/well in 96-well plates. Following a 12 h incubation, the cells were exposed to PSSF/BL-193 NAs at molar ratios of 1:0, 1:1, 1:3, 1:5, 1:7 or 1:9. After 48 h, the cells were co-incubated with MTT for 4 h, after which dimethyl sulfoxide (DMSO) was used to replace the old medium for dissolving the formazan produced by the cells. Lastly, the UV absorbance at 490 nm was quantified using a Thermo Scientific microplate reader. Finally, measuring the optimal sensitization ratio of PSSF and BL-193 through IC_{50} values.

After determining the optimal dose ratio, we measure the particle sizes and zeta potentials of PSSF/BL-193 NAs and PSSF NAs. Additionally, by staining with phosphotungstic acid, we observed the morphology of NAs using a transmission electron microscope (JEOL 100CX II, Japan).

2.4. *In vitro stability*

PSSF/BL-193 NAs and PSSF NAs at a concentration of 0.5 mg/ml, underwent separate incubation in PBS and PBS containing 10% FBS at 37 °C using a shaking incubator. The stability of these nanoparticles was assessed by monitoring changes in particle size at various time intervals using a ZetaSizer instrument. To enhance the formulation's stability during long-term storage and reduce transportation costs, we lyophilized 1 ml of a 1 mg/ml formulation with 10% sucrose as a cryoprotectant in a vacuum freeze-dryer. Post-lyophilization, the stability of the formulation was assessed by examining changes in particle size and morphological appearance upon reconstitution.

2.5. *Assembly mechanism*

Molecular docking was employed to elucidate the intermolecular forces within PSSF/BL-193 NAs. Furthermore, NaCl and SDS were employed to corroborate the presence of intermolecular forces in NAs. In a concise description, PSSF/BL-193 NAs were dispersed in NaCl (50 mM) and SDS (50 mM) solution, followed by incubation at 37 °C in an agitating chamber. The nanoparticle sizes were assessed at predefined time intervals using a ZetaSizer instrument.

2.6. *In vitro release patterns of PPT and BL-193*

We examined the release behaviors of PPT and BL-193 from PSSF/BL-193 NAs. To ensure complete dissolution of hydrophobic PPT and BL-193 released from NAs and facilitate detection, we added 20% THF to PBS (pH 7.4). PPT and BL-193 release were quantified at different time points using High-Performance Liquid Chromatography (HPLC) in the supplymentary Material.

2.7. *Cellular uptake*

4T1 cells were initially plated in 24-well plates and incubated for 12 h. Following this, the nutrient-free medium was exchanged with medium containing PSSF-Cy7 NAs, PSSF/BL-193-Cy7 NAs and Cy7 Sol (each at a concentration of 250 ng/ml of Cy7). After washing, fixing, or digesting, cell observations were conducted using CLSM or analyzed via flow cytometry (BD, East Rutherford, NJ, USA).

2.8. *Cytotoxicity*

The antiproliferative activities of the NAs was explored by MTT assay. 4T1 cells were plated in 96-well plates and incubated for 12 h. Then, nutrient free medium was discarded and the cells were treated with BL-193 Sol, PPT Sol, PPT/BL-193 Sol, PSSF NAs and PSSF/BL-193 NAs at uniform concentrations of PPT and/or BL-193 for 48 h. Subsequently, MTT solution was added, followed by a 4 h incubation period. Afterward, the well contents were aspirated, and 200 μl DMSO was introduced. Following a 10 min shaking period, the absorbance at 490 nm was quantified using a microplate reader.

2.9. *Cellular apoptosis*

4T1 cells were initially plated in 12-well plates and incubated for 12 h. Subsequently, the cells were treated with BL-193 Sol, PPT Sol, PPT/BL-193 Sol, PSSF NAs and PSSF/BL-193 NAs at uniform concentrations of PPT and/or BL-193, respectively. And then, the previous cell culture medium was collected into centrifuge tube. The cells were digested and then terminated by adding the old culture medium. The cells were centrifuged and suspended, and the supernatant was removed after another round of centrifugation. The cells were stained with the Annexin V-FITC Apoptosis Detection Kit. Subsequently, performed immediate flow cytometry analysis.

2.10. *Western blot assay*

4T1 cells were treated with BL-193 Sol, PPT Sol, PPT/BL-193 Sol, PSSF NAs, and PSSF/BL-193 NAs, all at matched concentrations of PPT and/or BL-193. The membranes were then blocked with 5% defatted milk prepared in TBST for 2 h. Subsequently, the PVDF membrane was separately incubated overnight at 4 °C with Bcl-2 rabbit monoclonal antibody and β-actin rabbit monoclonal antibody (highly diluted). It was then incubated with HRP-conjugated goat anti-rabbit IgG at room temperature for an additional 2 h. Intracellular Bcl-2 levels were observed using the ChemiDoc™ Imaging System.

2.11. *Pharmacokinetic*

Healthy SD rats weighing 200–220 g were employed for investigate the pharmacokinetic behavior of PSSF NAs and PSSF/BL-193 NAs *in vivo* ($n = 5$ per group). Specifically, Cy7 Sol and Cy7-labled NAs were administered at a dosage of 2 mg/kg Cy7 equivalent, were intravenously injected into the rats via the tail vein. Subsequently, blood samples were collected. Blood serum was obtained by centrifugation, and the blood serum concentrations of Cy7 were quantified.

2.12. *Biodistribution*

To assess the tumor-targeting capability of prodrug NAs, we utilized BALB/c mice bearing 4T1 tumors, with an

average tumor volume of 300 mm^3. Cy7 Sol and Cy7-labeled NAs were administered intravenously to mice. Following administration, fluorescence changes in the mice were monitored at set time intervals. Post-anesthesia, fluorescence intensities were quantified using an IVIS imaging system (PerkinElmer). Mice were euthanized and tumors as well as major organs were collected. Subsequently, we analyzed fluorescence intensities with the same IVIS imaging system.

2.13. *Hemolysis test*

Mouse blood was freshly collected, and serum was separated by centrifugation, followed by washing with saline to isolate erythrocytes. We then introduced BL-193 Sol, PPT Sol, PPT/BL-193 Sol, PSSF NAs and PSSF/BL-193 NAs, all at equivalent concentrations of PPT and/or BL-193, into equal amounts of erythrocytes suspensions. Following a 3 h incubation at 37 °C on a shaker, we measured the absorbance at 545 nm.

2.14. *Antitumor efficacy*

To establish the tumor-bearing model, 4T1 cells suspensions were subcutaneously injected into the mice. Mice were randomly allocated into six groups upon the tumor size reached 100 mm^3, each consisting of five individuals: control group (PBS), BL-193 Sol, PSSF/BL-193 Sol, PPT Sol, PSSF NAs and PSSF/BL-193 NAs. These formulations were administered every other day for a total of five administrations, with each containing equivalent concentrations of PPT (4 mg/kg) and/or BL-193 (25 mg/kg). Four days following the final treatment session, blood samples were collected, and the mice were euthanized to acquire the major organs and tumor tissues. The organs and tumors were immersed in 4% paraformaldehyde for H&E staining and TUNEL assay.

3. Results and discussion

3.1. *BL-193-mediated chemotherapy sensitization*

This project commenced with an interesting finding that BL-193 at non-cytotoxic dose exhibited the remarkable ability to improve the chemotherapy sensitivity of breast cancer cells to PPT (Fig. 2A). As depicted in Fig. 2B, BL-193 alone demonstrated weak cytotoxicity and failed to induce cellular demise even at a concentration of 2 μM. Interestingly, the cytotoxicity of PPT against 4T1 cells was remarkably enhanced when BL-193 was introduced at a non-cytotoxic concentration of 500 nM (Fig. 2C and Table S1). Furthermore, given the severe non-specific toxicity of PPT, a redox-sensitive prodrug (PSSF) of PPT was rationally designed and synthesized by coupling 9-fluorenyl-methanol (Fmoc-OH) with PPT linked via disulfide bond according to our previous work (Fig. S1). The chemical structure of PSSF was confirmed by MS and ^1H NMR, respectively (Figs. S2-S3). Similarly, BL-193 also enhanced the sensitivity of 4T1 cells to PSSF (Fig. 2D and Tab.le S2). Additionally, to further confirm the toxicity reduction attributed to the prodrug strategy, mouse embryonic fibroblasts (3T3 cells) were employed to assess cytotoxicity. As shown in Fig. 2E and Table S3, PSSF exhibited significantly lower cytotoxicity against 3T3 cells in comparison to PPT, with IC_{50} values increased by more than 40-folds. Significantly, BL-193 showed negligible sensitization to PPT or PSSF on 3T3 cells (Fig. 2E), demonstrating that BL-193 can achieve tumor-specific sensitization without additional systemic toxicity.

3.2. *Preparation and characterization of nanoassemblies*

Given the remarkable chemotherapy sensitization effect of BL-193 on PSSF, we attempted to prepare PSSF/BL-193 NAs to achieve synchronous delivery using small molecule co-assembly nanotechnology. As shown in Table S4, BL-193 and PSSF could co-assemble into NAs at various molar ratios ranging from 1:0 to 1:9. Subsequently, in order to determine the optimal PSSF/BL-193 ratio for subsequent studies, we examined the cytotoxic effects of NAs with different molar ratios on 4T1 cells. As shown in Fig. S4, PSSF/BL-193 NAs at a PSSF/BL-193 ratio of 1:5 exhibited the strongest cytotoxicity against 4T1 cells.

Based on the above findings, we prepared PSSF/BL-193 NAs with a PSSF/BL-193 molar ratio of 1:5 (Fig. 3A). Moreover, the self-assembled PSSF NAs without BL-193 was prepared as the control NAs. As shown in Figs. 3B-3C, S5 and Table S5, both PSSF NAs and PSSF/BL-193 NAs exhibited uniform particle sizes of ~ 85 nm. Transmission electron microscope (TEM) images further confirmed their regular spherical structures (Fig. S7). Furthermore, the incorporation of DSPE-PEG_{2K} endowed NAs with a negative potential of about −25 mV, which contributed to reduce plasma protein adsorption and prolong blood circulation (Fig. S6). The colloidal stability of PSSF NAs and PSSF/BL-193 NAs was assessed through co-incubation with PBS (pH 7.4) or PBS containing 10% FBS, respectively. Both PSSF NAs and PSSF/BL-193 NAs demonstrated stability with no significant changes in particle size (Figs. 3D and S8). For long-term stable storage, the nanoassemblies were lyophilized and subsequently reconstituted. As shown in Fig. S9-S10, there was no discernible cake collapse in the lyophilized samples, and the particle size of the NAs remained relatively unchanged after reconstitution compared to their pre-freeze-drying state.

3.3. *Nanoassembly mechanism*

We subsequently explored the nanoassembly mechanisms of the PSSF/BL-193 nanoassemblies (NAs). Utilizing the molecular docking technique, we delved into the driving forces behind the nanoassembly between PSSF and BL-193. As depicted in Fig. 3E, hydrophobic interaction and π-π stacking emerged as the primary driving forces in the nanoassembly of PSSF and BL-193. To experimentally validate the theoretical calculations, SDS and NaCl were employed to disrupt hydrophobic interaction and electrostatic interaction in the nanoassemblies, respectively. As illustrated in Fig. S11, the particle sizes of PSSF/BL-193 NAs exhibited a significant increase in the presence of SDS, while NaCl had only a marginal impact on the NAs under identical conditions. This

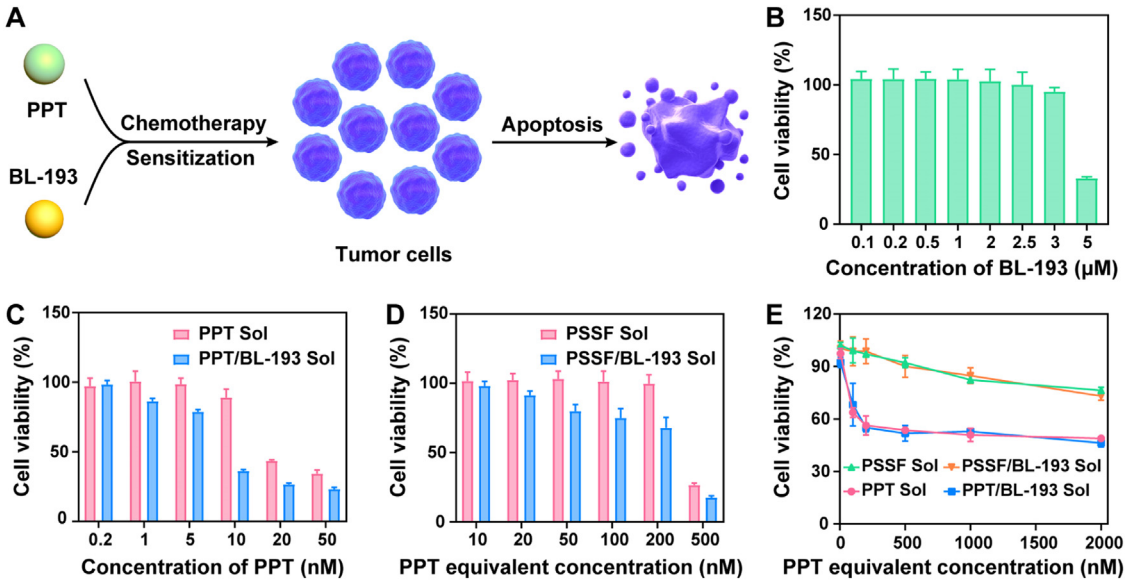

Fig. 2 – BL-193-mediated chemotherapy sensitization. (A) Schematic illustration of the sensitization of BL-193 and PPT; (B) *In vitro* cytotoxicity against 4T1 cells treated with BL-193 Sol; (C) Cytotoxicity of PPT Sol or PPT/BL-193 Sol against 4T1 cells; (D) Cytotoxicity of PSSF Sol or PSSF/BL-193 Sol against 4T1 cells; (E) Cytotoxicity of PPT Sol, PPT/BL-193 Sol, PSSF Sol and PSSF/BL-193 Sol against 3T3 cells.

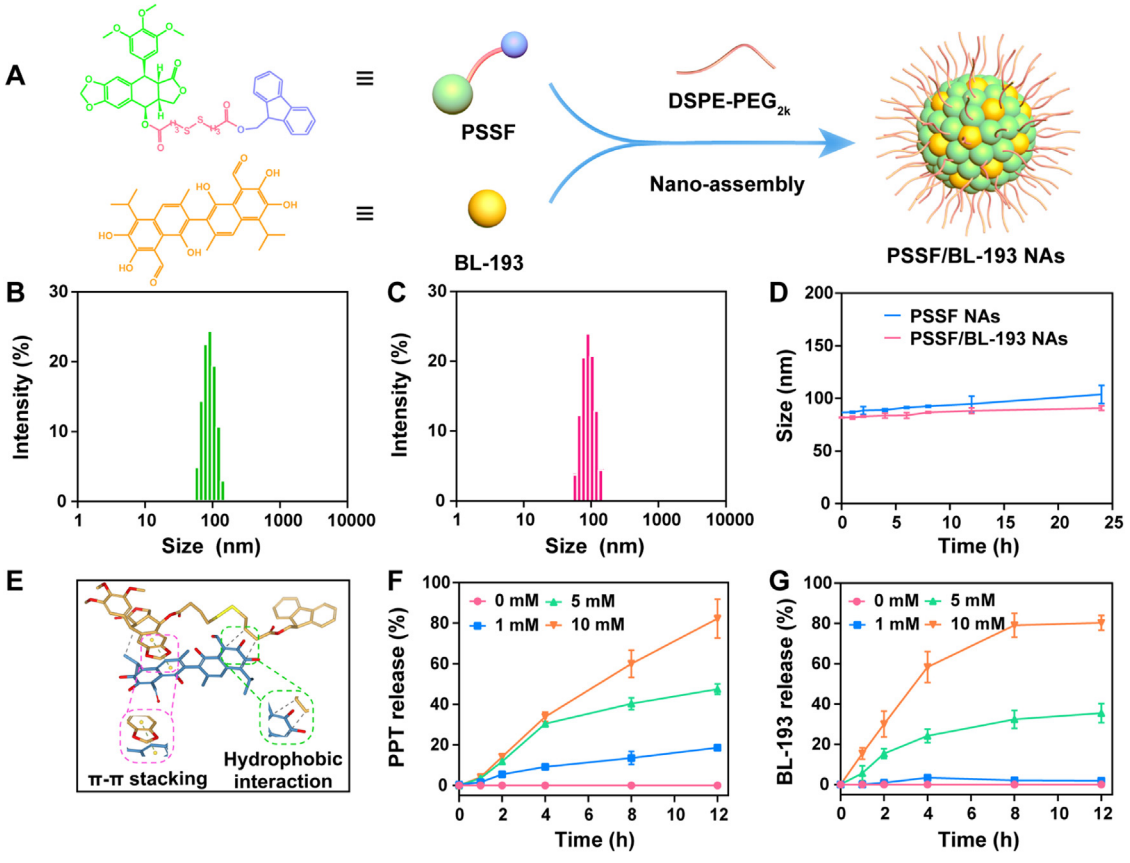

Fig. 3 – Preparation and characterization of nanoassemblies. (A) Scheme of nanoassembly process between PSSF and BL-193; (B) The size distribution of PSSF NAs; (C) The size distribution of PSSF/BL-193 NAs; (D) Colloidal stability of PSSF NAs and PSSF/BL-193 NAs incubated in PBS (pH 7.4); (E) Molecular docking simulation of PSSF and BL-193; (F) Cumulative release of PPT from PSSF/BL-193 NAs with 0 mM, 1 mM, 5 mM and 10 mM DTT (n = 3); (G) Cumulative release of BL-193 from PSSF/BL-193 NAs with 0 mM, 1 mM, 5 mM and 10 mM DTT (n = 3).

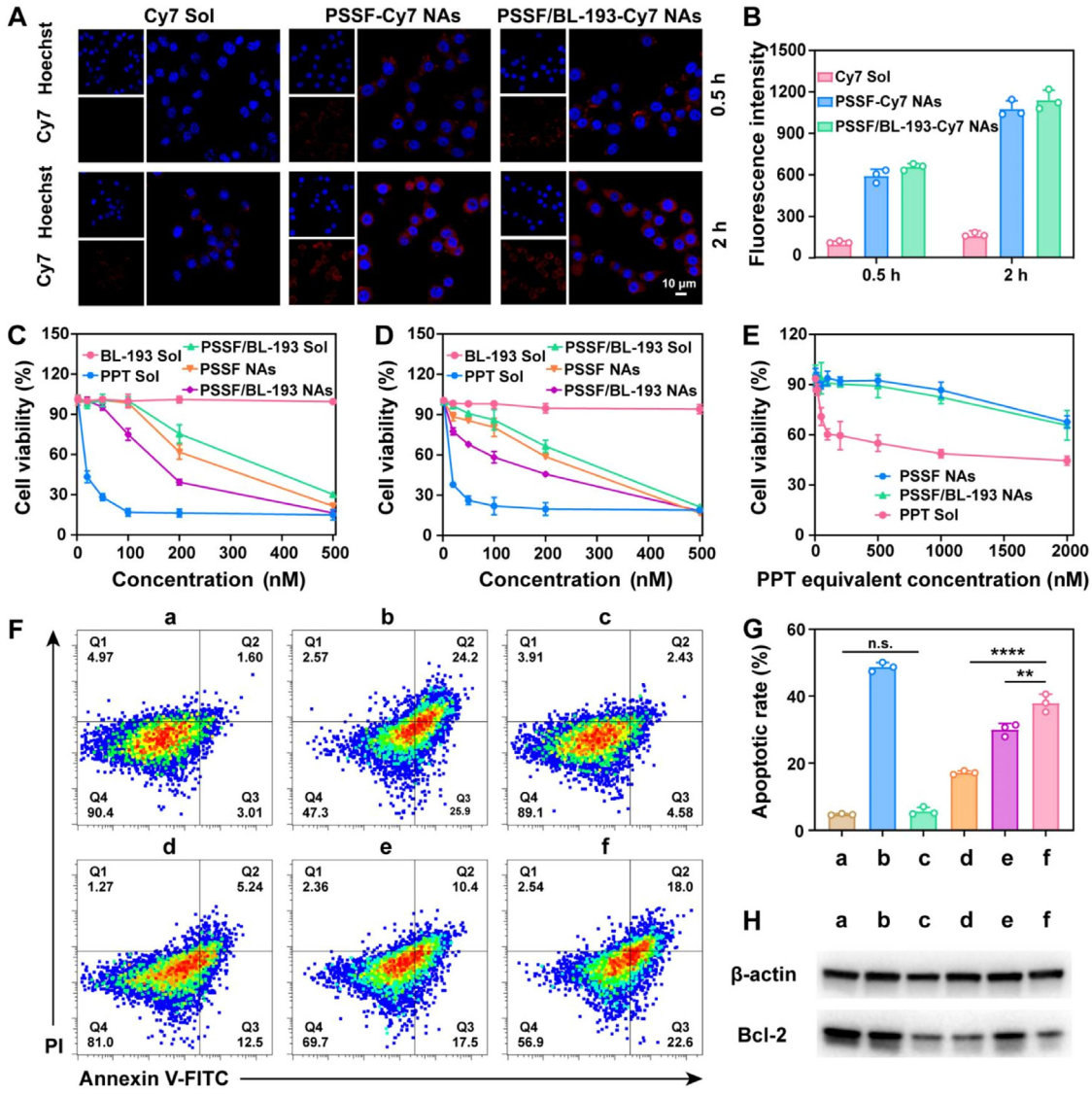

Fig. 4 – *In vitro* cytotoxicity and sensitization mechanism. Cellular uptake after incubation in 4T1 cells at 0.5 h and 2 h by CLSM (A) and flow cytometry (B); (C) *In vitro* cytotoxicity against 4T1 cells (D), RM-1 cells (E) and 3T3 cells treated with various formulations; (F) Cellular apoptosis of 4T1 cells by flow cytometry using Annexin V FITC/PI Apoptosis Kit; (G) Quantitative analysis of cellular apoptosis; (H) Western blotting image of Bcl-2 protein expression in 4T1 cells. (a: control, b: PPT Sol, c: BL-193 Sol, d: PPT/BL-193 Sol, e: PSSF NAs, f: PSSF/BL-193 NAs).

observation suggests that hydrophobic forces play a pivotal role in the assembly process.

3.4. *Drug release*

As mentioned earlier, the introduction of disulfide bond was expected to accelerate drug release in GSH-overexpressed tumor cells (Fig. S12). To explore this, we investigated the *in vitro* drug release by quantifying the release of PPT and BL-193 from PSSF/BL-193 NAs in the presence or absence of DTT (a surrogate for GSH). As shown in Fig. 3F, the release of PPT was accelerated in a concentration-dependent manner in the presence of DTT. As the DTT concentration increased, the release of PPT became faster, with over 80% of PPT being released within 12 h in the presence of 10 mM DTT. Additionally, the release of BL-193 was also accelerated in the presence of DTT, exhibiting simultaneous release with PPT (Fig. 3G). This can be attributed to the disulfide bond breakage, which promoted the disintegration of PSSF/BL-193 NAs. Furthermore, both PPT and BL-193 showed slow drug release in the absence of DTT, demonstrating the characteristic of tumor-specific drug release (Fig. 3F-3G).

3.5. *Cellular uptake*

High cell uptake efficiency is essential for tumor intracellular stimuli-responsive drugs. The cellular uptake was investigated by assessing the intracellular fluorescence signals of Cy7-labled NAs in 4T1 cells, using both CLSM

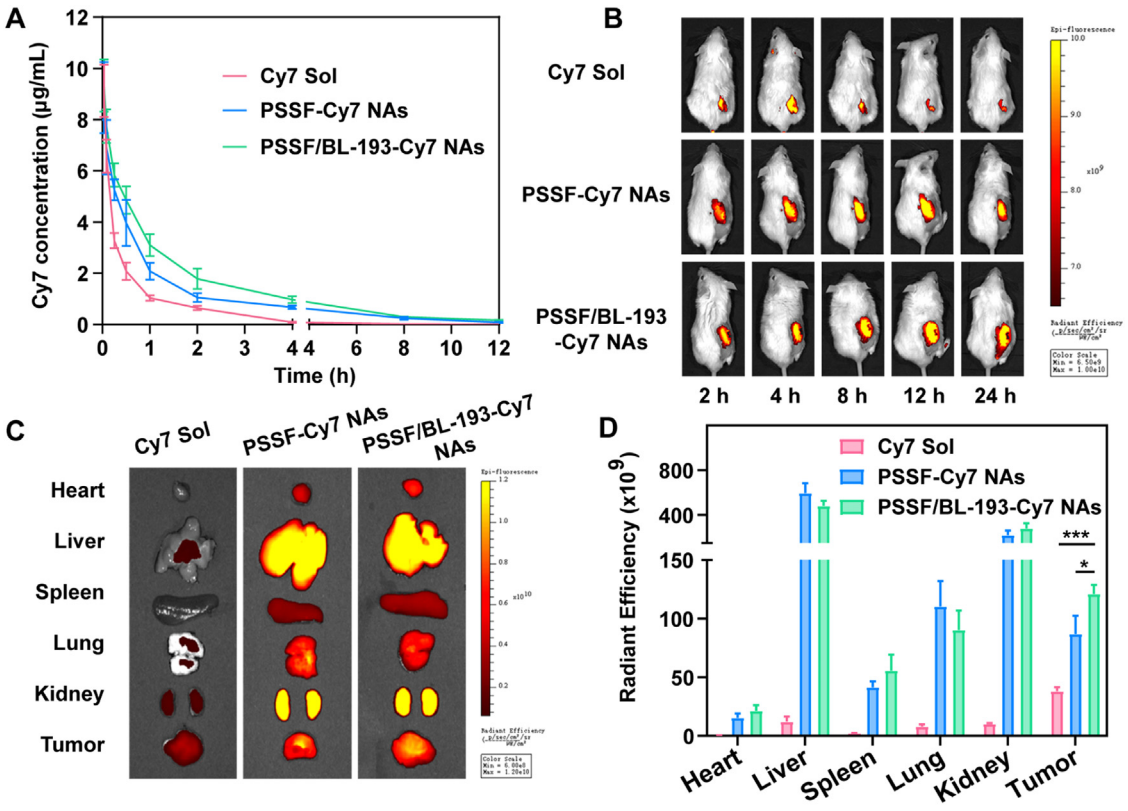

Fig. 5 – Pharmacokinetics and biodistribution. (A) The pharmacokinetic behaviors of Cy7 Sol, PSSF-Cy7 NAs and PSSF/BL-193-Cy7 NAs; (B) Living images of 4T1 tumor-bearing BALB/c mice treated with various formulations; (C) *Ex vivo* images of major organs and tumors after injection of various formulations; (D) Quantification of the average fluorescence intensity of *ex vivo* images of major organs and tumors ($n = 3$).

imaging and flow cytometry analysis. As depicted in Fig. 4A-4B, the cellular uptake of Cy7 Sol and Cy7-labled NAs exhibited a time-dependent increase, with Cy7-labled NAs demonstrating significantly higher cellular uptake than Cy7 Sol both at 0.5 and 2 h. Moreover, there was no notable distinction between PSSF NAs and PSSF/BL-193 NAs, which was attributed to their similar particle size and surface properties.

3.6. *In vitro cytotoxicity and sensitization mechanism*

BL-193-mediated chemotherapy sensitization, reduction-responsive drug release characteristics and high-efficiency cellular uptake provide the possibility to improve the cytotoxicity of nanoassemblies. To test our hypothesis, BL-193-sensitized cytotoxicity of nanoassemblies was evaluated using 4T1 cells through an MTT assay. As shown in Fig. 4C and Table S8, BL-193 alone displayed negligible cytotoxicity against 4T1 cells. However, PSSF/BL-193 NAs showed higher cytotoxicity compared to PSSF NAs due to the tumor-specific chemotherapy sensitization mediated by BL-193, even within a non-toxic concentration range. The PSSF/BL-193 Sol only exhibited moderate cytotoxicity, possibly attributed to the asynchronous and low cellular uptake behavior of PSSF and BL-193. Furthermore, similar results were observed in an MTT assay conducted on RM-1 cells (Fig. 4D and Table S8). In addition, PSSF NAs demonstrated lower cytotoxicity compared to PPT Sol in 3T3 cells, highlighting the significant advantage of prodrug strategies in alleviating the toxic side effects of PPT. Interestingly, PSSF NAs and PSSF/BL-193 NAs exhibited comparable cytotoxicity in 3T3 cells, demonstrating the tumor-specific chemotherapy sensitization of BL-193 (Fig. 4E and Table S9). Next, the cellular apoptosis was examined through the Annexin V FITC/PI Apoptosis Kit using flow cytometry following various treatments. Consistent with the cell viability outcomes obtained through the MTT assay, a notable increase in the percentage of apoptotic cells was observed in the PSSF/BL-193 NAs group (greater than 50%) compared to the BL-193 Sol, PSSF NAs, and PSSF/BL-193 Sol groups (Fig. 4F-4G). Taken together, these results highlighted the benefits of BL-193-mediated chemotherapy sensitization with tumor-specific characteristics and nanoassembly-mediated synchronous delivery in enhancing anti-tumor effects *in vitro*.

In view of the excellent performance of BL-193 in sensitizing cytotoxicity, we delved into its potential mechanisms. Existing research suggests that cellular apoptosis is intricately regulated by intracellular anti-apoptotic and pro-apoptotic factors. Certain anti-apoptotic factors (such as Bcl-2) are commonly overexpressed in most tumor cells, aiding in their resistance to apoptosis [41]. Notably, previous studies have reported that BL-193 has the ability to inhibit the cellular expression of Bcl-2 [42–44]. Therefore, we postulated that the significantly increased

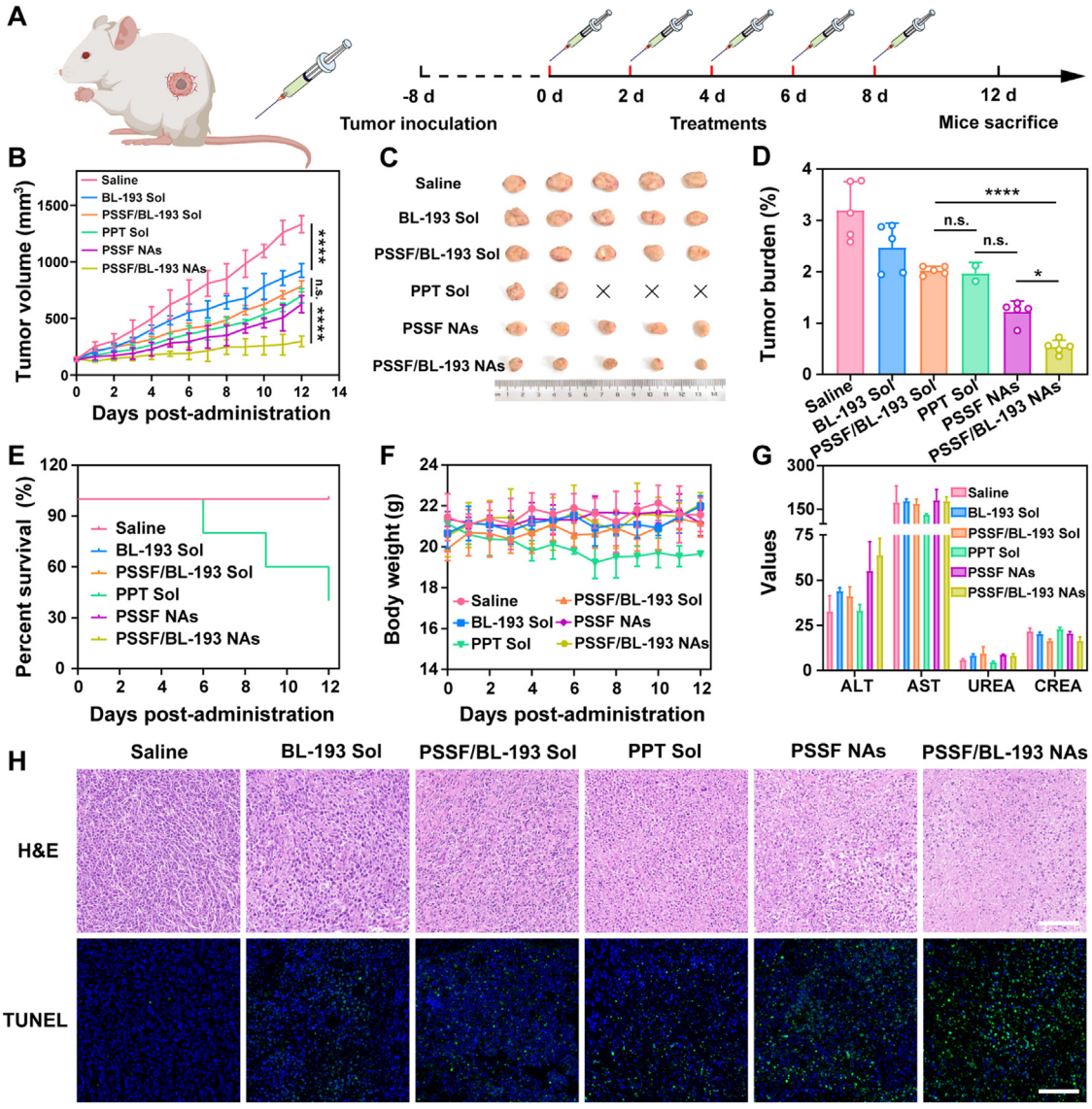

Fig. 6 – *In vivo* antitumor evaluation. (A) Treatment schedule; (B) Tumor growth profiles after various treatments ($n = 5$); (C) Tumors images; (D) Tumor burden after treatments; (E) Mice percent survival during treatments ($n = 5$); (F) Changes in body weight during treatments ($n = 5$); (G) Hepatic and renal function indicators of mice-bearing tumor after the last treatment. (H) H&E and TUNEL staining images of tumors after various treatments. Scale bar = 100 μm.

cellular apoptosis in the presence of BL-193 can be attributed to the down-regulation of intracellular Bcl-2 protein. To investigate this, we employed the Western Blot assay to examine the expression of Bcl-2 protein in 4T1 cells subjected to various treatments. Fig. 4H illustrates that formulations incorporating BL-193 (including BL-193 Sol, PPT/BL-193 Sol, and PSSF/BL-193 NAs) significantly diminished Bcl-2 expression. This finding suggests that BL-193 effectively down-regulates Bcl-2 protein levels.

3.7. *Pharmacokinetics*

Pharmacokinetics plays a pivotal role in evaluating *in vivo* delivery efficiency, exerting a profound impact on biodistribution and the final anti-tumor effectiveness. Therefore, we conducted an investigation into the pharmacokinetic profiles of NAs in SD rats. To facilitate measurement and visualization of distribution in the body, Cy7-labeled DSPE-PEG_{2k} was used to prepare PEGylated NAs (PSSF-Cy7 NAs and PSSF/BL-193-Cy7 NAs). The pharmacokinetic behavior of NAs *in vivo* was indicated by detecting the fluorescence signal of Cy7. The drug concentration-time curves (AUC) and primary pharmacokinetic parameters were presented in the Fig. 5A and Table S10. Cy7 Sol demonstrated rapid blood clearance within 4 h. At the same Cy7 dose, PSSF-Cy7 NAs and PSSF/BL-193-Cy7 NAs exhibited longer circulation times in the bloodstream, resulting in increased AUC by 2.3 and 3.2 times, respectively. In addition, PSSF/BL-193-Cy7 NAs showed better pharmacokinetic behavior than PSSF-Cy7 NAs, possibly due to the introduction of BL-193 to enhance the stability of the NAs (Fig. S8).

3.8. *Biodistribution*

Good pharmacokinetic behavior will help increase the accumulation of NAs at the tumor site via the EPR effect. We subsequently evaluated the biodistribution of Cy7 Sol, PSSF-Cy7 NAs and PSSF/BL-193-Cy7 NAs in 4T1 breast tumor-bearing mice. As shown in Figs. 5B and S13, Cy7 Sol achieved maximum accumulation at the tumor site at 4 h after administration, while PSSF-Cy7 NAs and PSSF/BL-193-Cy7 NAs reached peak tumor accumulation at 12 h, attributed to their distinct pharmacokinetic behavior. In addition, PSSF-Cy7 NAs and PSSF/BL-193-Cy7 NAs exhibited higher tumor accumulation than Cy7 Sol at any time point due to the prolonged blood circulation time of NAs (Fig. S13). For more accurate quantification, major organs and tumors were isolated at the maximum accumulation time point, and *ex vivo* tumor distribution was conducted (Fig. 5C-5D). Notably, PSSF/BL-193-Cy7 NAs demonstrated higher fluorescence signals at the tumor site compared to PSSF-Cy7 NAs, aligning with the pharmacokinetic profiles (Fig. 5A).

3.9. *In vivo antitumor activity*

After elaborated design, synthesis, preparation, and a comprehensive series of characterizations, the PSSF/BL-193 NAs exhibited excellent *in vitro* properties and *in vivo* delivery efficiency. These features encompassed excellent stability, good chemotherapy sensitization, reduced toxicity, favorable pharmacokinetic properties, and improved tumor accumulation. It is anticipated that these attributes will significantly enhance PPT-mediated chemotherapy *in vivo*. Consequently, a xenograft model of 4T1 breast cancer in BALB/c mice was established to assess the *in vivo* antitumor efficacy of NAs (Fig. 6A). As shown in Fig. 6B-6D, BL-193 Sol, PSSF/BL-193 Sol and PPT Sol demonstrated inferior antitumor efficiency, attributed to rapid blood clearance and insufficient tumor accumulation. In contrast, PSSF NAs exerted more potent tumor growth inhibition than PPT Sol due to enhanced tumor accumulation, primarily due to enhanced tumor accumulation, although no significant difference was observed between them (Fig. 6D). The main reason for this may be attributed to delayed and insufficient prodrug activation. As anticipated, PSSF/BL-193 NAs effectively suppressed tumor progression and exhibited the highest anti-tumor efficiency compared to PSSF NAs. This enhanced efficacy can be attributed to BL-193-mediated chemotherapy sensitization and higher tumor accumulation. In addition, the results of H&E and TUNEL staining at tumor site also revealed that the PSSF/BL-193 NAs induced a higher level of tumor apoptosis (Fig. 6H).

During the course of treatment, the mice in the PPT group died, and there was a significant decrease in the body weight of the mice, suggesting substantial systemic toxicity associated with PPT. In contrast, the survival and weight of mice in the PPT prodrug group (including PSSF/BL-193 Sol, PSSF NAs and PSSF/BL-193 NAs) remained stable. Additionally, PSSF/BL-193 NAs did not induce significant changes in hepatorenal function parameters (Fig. 6G), hemolysis (Fig. S14), or H&E staining of the main organs (Fig. S15). These results collectively indicate that the prodrug strategy effectively mitigates system toxicity. In general, these results demonstrated that BL-193-empowered prodrug nanoassembly could act as an efficient and safe combination treatment paradigm for precision cancer chemotherapy for tumor therapy.

4. Conclusion

In summary, we explored a novel chemotherapy paradigm by combining prodrug strategy and chemotherapy sensitization using molecular nanoassembly techniques, thereby amplifying the chemotherapy efficacy-toxicity benefit. Specifically, the elaborate design and synthesis of PTT prodrug addressed the serious systemic toxicity issues associated with PTT, substantially improving its tolerability. Concurrently, BL-193-mediated chemotherapy sensitization improved the therapeutic efficiency of the PPT prodrug, particularly addressing the challenge of delayed and insufficient prodrug activation. Importantly, BL-193-mediated chemotherapy sensitization demonstrated excellent selectivity between normal and tumor cells, enhancing the elimination of tumor cells without adversely affecting the toxicity of normal cells. A series of evaluations demonstrated the significant potential of PSSF/BL-193 NAs in achieving highly efficient tumor elimination with low off-target toxicity. This marks the first attempt to intelligently address the issue of poor chemotherapy efficacy resulting from prodrug activation through a unique chemotherapy sensitization approach. This study provides a new combination therapy model for tumor precision chemotherapy.

Conflicts of interest

The authors declare that there is no conflicts of interest.

Acknowledgements

This work was financially supported by the Basic Research Projects of Liaoning Provincial Department of Education (LJKZZ20220109), the Shenyang Youth Science and Technology Innovation Talents Program (No. RC210452), the National Natural Science Foundation of China (No. 82204317) and the Natural Science Foundation of Liaoning Province (No. 2022-BS-162).

Supplementary materials

Supplementary material associated with this article can be found, in the online version, at doi:10.1016/j.ajps.2024.100892.

References

[1] Siegel RL, Miller KD, Jemal A. Cancer statistics, 2020. CA Cancer J Clin 2020;70(1):7–30.

[2] Kaur R, Bhardwaj A, Gupta S. Cancer treatment therapies: traditional to modern approaches to combat cancers. Mol Biol Rep 2023;50(11):9663–76.
[3] Hassan S, Prakash G, Ozturk A, Saghazadeh S, Sohail MF, Seo J, et al. Evolution and clinical translation of drug delivery nanomaterials. Nano Today 2017;15:91–106.
[4] Turajlic S, Sottoriva A, Graham T, Swanton C. Resolving genetic heterogeneity in cancer. Nat Rev Genet 2019;20(7):404–16.
[5] Li H, Wei W, Xu H. Drug discovery is an eternal challenge for the biomedical sciences. Acta Materia Medica 2022;1(1): 1–3.
[6] Luo C, Sun J, Sun B, Liu D, Miao L, Goodwin TJ, et al. Facile fabrication of tumor redox-sensitive nanoassemblies of small-molecule oleate prodrug as potent chemotherapeutic nanomedicine. Small 2016;12(46):6353–62.
[7] Pisa R, Kapoor TM. Chemical strategies to overcome resistance against targeted anticancer therapeutics. Nat Chem Biol 2020;16(8):817–25.
[8] Bianchini G, Balko JM, Mayer IA, Sanders ME, Gianni L. Triple-negative breast cancer: challenges and opportunities of a heterogeneous disease. Nat Rev Clin Oncol 2016;13(11):674–90.
[9] Chen Y, Zhao T, Bai M, Gu T, Sun J, He Z, et al. Emerging small molecule-engineered hybrid nanomedicines for cancer therapy. Chem Eng J 2022;435:135160.
[10] Miranda-Vera C, Hernández ÁP, García-García P, Díez D, García PA, Castro MÁ. Podophyllotoxin: recent advances in the development of hybridization strategies to enhance its antitumoral profile. Pharmaceutics 2023;15(12):2728.
[11] Shi RJ, Fan HY, Yu XH, Tang YL, Jiang J, Liang XH. Advances of podophyllotoxin and its derivatives: patterns and mechanisms. Biochem Pharmacol 2022;200:115039.
[12] Shah Z, Gohar UF, Jamshed I, Mushtaq A, Mukhtar H, Zia-Ui-Haq M, et al. Podophyllotoxin: history, recent advances and future prospects. Biomolecules 2021;11(4):603.
[13] Yin M, Fang Y, Sun X, Xue M, Zhang C, Zhu Z, et al. Synthesis and anticancer activity of podophyllotoxin derivatives with nitrogen-containing heterocycles. Front Chem 2023;11:1191498.
[14] Zhao W, Cong Y, Li HM, Li S, Shen Y, Qi Q, et al. Challenges and potential for improving the druggability of podophyllotoxin-derived drugs in cancer chemotherapy. Nat Prod Rep 2021;38(3):470–88.
[15] Jin L, Song Z, Cai F, Ruan L, Jiang R. Chemistry and biological activities of naturally occurring and structurally modified podophyllotoxins. Molecules 2022;28(1):302.
[16] Xiao J, Gao M, Sun Z, Diao Q, Wang P, Gao F. Recent advances of podophyllotoxin/epipodophyllotoxin hybrids in anticancer activity, mode of action, and structure-activity relationship: an update (2010-2020). Eur J Med Chem 2020;208: 112830.
[17] Yang F, Zhao Z, Sun B, Chen Q, Sun J, He Z, et al. Nanotherapeutics for antimetastatic treatment. Trends Cancer 2020;6(8):645–59.
[18] Linares J, Sallent-Aragay A, Badia-Ramentol J, Recort-Bascuas A, Mendez A, Manero-Ruperez N, et al. Long-term platinum-based drug accumulation in cancer-associated fibroblasts promotes colorectal cancer progression and resistance to therapy. Nat Commun 2023;14(1):746.
[19] Li S, Shan X, Wang Y, Chen Q, Sun J, He Z, et al. Dimeric prodrug-based nanomedicines for cancer therapy. J Control Release 2020;326:510–22.
[20] Wang Y, Luo C, Zhou S, Wang X, Zhang X, Li S, et al. Investigating the crucial roles of aliphatic tails in disulfide bond-linked docetaxel prodrug nanoassemblies. Asian J Pharm Sci 2021;16(5):643–52.
[21] Santra S, Kaittanis C, Santiesteban OJ, Perez JM. Cell-specific, activatable, and theranostic prodrug for dual-targeted cancer imaging and therapy. J Am Chem Soc 2011;133(41):16680–8.
[22] Li G, Sun B, Li Y, Luo C, He Z, Sun J. Small-molecule prodrug nanoassemblies: an emerging nanoplatform for anticancer drug delivery. Small 2021;17(52):e2101460.
[23] Luo C, Sun J, Liu D, Sun B, Miao L, Musetti S, et al. Self-assembled redox dual-responsive prodrug-nanosystem formed by single thioether-bridged paclitaxel-fatty acid conjugate for cancer chemotherapy. Nano Lett 2016;16(9):5401–8.
[24] Yu W, Shevtsov M, Chen X, Gao H. Advances in aggregatable nanoparticles for tumor-targeted drug delivery. Chin Chem Lett 2020;31(6):1366–74.
[25] Luo C, Sun B, Wang C, Zhang X, Chen Y, Chen Q, et al. Self-facilitated ROS-responsive nanoassembly of heterotypic dimer for synergistic chemo-photodynamic therapy. J Control Release 2019;302:79–89.
[26] Kong X, Qi Y, Wang X, Jiang R, Wang J, Fang Y, et al. Nanoparticle drug delivery systems and their applications as targeted therapies for triple negative breast cancer. Prog Mater Sci 2023;134:101070.
[27] Zhang H, Wang J, Han R, Sun B, Luo C. Bioorthogonal chemistry-driven anticancer nanotherapeutics. Trends Chem 2023;5(9):697–710.
[28] Llop J, Lammers T. Nanoparticles for cancer diagnosis, radionuclide therapy and theranostics. ACS Nano 2021;15(11):16974–81.
[29] Chen Q, Liu G, Liu S, Su H, Wang Y, Li J, et al. Remodeling the tumor microenvironment with emerging nanotherapeutics. Trends Pharmacol Sci 2018;39(1):59–74.
[30] Wang C, Yu H, Yang X, Zhang X, Wang Y, Gu T, et al. Elaborately engineering of a dual-drug co-assembled nanomedicine for boosting immunogenic cell death and enhancing triple negative breast cancer treatment. Asian J Pharm Sci 2022;17(3):412–24.
[31] Blanco E, Shen H, Ferrari M. Principles of nanoparticle design for overcoming biological barriers to drug delivery. Nat Biotechnol 2015;33(9):941–51.
[32] Wang Z, Zhang S, Kong Z, Li S, Sun J, Zheng Y, et al. Self-adaptive nanoassembly enabling turn-on hypoxia illumination and periphery/center closed-loop tumor eradication. Cell Rep Med 2023;4(4):101014.
[33] He M, Yu L, Yang Y, Zou B, Ma W, Yu M, et al. Delivery of triptolide with reduction-sensitive polymer nanoparticles for liver cancer therapy on patient-derived xenografts models. Chin Chem Lett 2020;31(12):3178–82.
[34] He X, Chen X, Liu L, Zhang Y, Lu Y, Zhang Y, et al. Sequentially triggered nanoparticles with tumor penetration and intelligent drug release for pancreatic cancer therapy. Adv Sci 2018;5(5):1701070.
[35] Liu Y, Wang X, Wang Z, Liao R, Qiu Q, Wang Y, et al. Reduction-responsive stearyl alcohol-cabazitaxel prodrug nanoassemblies for cancer chemotherapy. Pharmaceutics 2023;15(1):262.
[36] Wang Y, Li S, Wang X, Chen Q, He Z, Luo C, et al. Smart transformable nanomedicines for cancer therapy. Biomaterials 2021;271:120737.
[37] Yang F, Ji Q, Liao R, Li S, Wang Y, Zhang X, et al. Precisely engineering a dual-drug cooperative nanoassembly for proteasome inhibition-potentiated photodynamic therapy. Chin Chem Lett 2022;33(4):1927–32.
[38] Chen F, Fang Y, Chen X, Deng R, Zhang Y, Shao J. Recent advances of sorafenib nanoformulations for cancer therapy: smart nanosystem and combination therapy. Asian J Pharm Sci 2021;16(3):318–36.
[39] Wang X, Wang Y, Yu J, Qiu Q, Liao R, Zhang S, et al. Reduction-hypersensitive podophyllotoxin prodrug self-

assembled nanoparticles for cancer treatment. Pharmaceutics 2023;15(3):784.
[40] Li Y, Li L, Jin Q, Liu T, Sun J, Wang Y, et al. Impact of the amount of PEG on prodrug nanoassemblies for efficient cancer therapy. Asian J Pharm Sci 2022;17(2):241–52.
[41] Zhang L, Lu Z, Zhao X. Targeting Bcl-2 for cancer therapy. Biochim Biophys Acta Rev Cancer 2021;1876(1):188569.
[42] Paunovic D, Rajkovic J, Novakovic R, Grujic-Milanovic J, Mekky RH, Popa D, et al. The potential roles of gossypol as anticancer agent: advances and future directions. Chin Med 2023;18(1):163.
[43] Wong FY, Liem N, Xie C, Yan FL, Wong WC, Wang L, et al. Combination therapy with gossypol reveals synergism against gemcitabine resistance in cancer cells with high BCL-2 expression. PLoS One 2012;7(12):e50786.
[44] Zeng Y, Liu H, Ma J, Li K, Chang P, Wang C, et al. Cobalt ferrite-gossypol coordination nanoagents with high photothermal conversion efficiency sensitizing chemotherapy against Bcl-2 to induce tumor apoptosis. Small 2023;19(34):e2300104.